

THEORY OF PHOTOSPHERIC EMISSION FROM RELATIVISTIC OUTFLOWS

R. RUFFINI, I. A. SIUTSOU AND G. V. VERESHCHAGIN

ICRANet, 65122, p.le della Repubblica, 10, Pescara, Italy and
ICRA and Dipartimento di Fisica, Università di Roma “Sapienza”, 00185, p.le A. Moro 5, Rome, Italy
Draft version November 6, 2018

ABSTRACT

Two popular models of optically thick relativistic outflows exist: the wind and the shell. We propose a unified treatment of photospheric emission within these models. We show that quite counterintuitive situations may appear when e.g. geometrically thin shell may behave as thick wind. For this reason we introduce notions of photon thick and photon thin outflows. They appear more general and better physically motivated than winds and shells when photospheric emission is considered.

We obtain light curves and observed spectra for both photon thick and photon thin outflows. In the photon thick case we generalize the results obtained for steady wind. It is our main finding that the photospheric emission from the photon thin outflow is dominated by diffusion and produces non thermal time integrated spectra, which may be described by the Band function well known in the GRB literature.

Energetic GRBs should produce photon thin outflows and therefore when only time integrated spectra for such GRBs are available we naturally expect them to have a Band shape. In the literature Band spectra for the photospheric emission of GRBs are obtained only involving additional dissipative mechanisms which are not required here.

Subject headings: Opacity — Plasmas — Radiation mechanisms: thermal — X-rays: bursts

1. INTRODUCTION

High Lorentz factors of the bulk motion of various outflows are common in relativistic astrophysics. The best known examples are Active Galactic Nuclei (Maraschi 2003), microquasars and Gamma-Ray Bursts (GRBs) (Piran 2004). In the latter case outflows indeed reach ultrarelativistic velocities.

Various models are suggested to explain the acceleration of outflows to ultrarelativistic velocities. The electromagnetic model (Lyutikov 2006) assumes that the energy in the source of GRB is converted into electromagnetic energy which is transported in the form of a Poynting flux. We adopt here another popular idea that the energy release leads to creation of an optically thick source which expands due to thermal acceleration. This idea is the basis of both the fireball (Piran (1999, 2004) and references therein) and the fireshell (Ruffini et al. (2001, 2009) and references therein) models.

In pioneer works by Goodman (1986) who considered an instant explosion, and by Paczynski (1986) who discussed a gradual energy release, a conclusion was reached that the electron-positron plasma is created in the source of GRB. Assuming further that the plasma reaches thermal equilibrium they focused on hydrodynamic expansion in such models and gave photometric and spectroscopic predictions for GRBs. Later, baryonic loading of fireballs was considered for explosions by Shemi & Piran (1990) and for winds by Paczynski (1990). Abramowicz et al. (1991) considered the appearance of the photosphere of the relativistic wind to a distant observer showing that its shape is concave.

The interest in photospheric emission from relativistic winds has been revived recently in papers by Daigne & Mochkovitch (2002), Pe’er et al. (2007), Beloborodov (2011), Ryde et al. (2011a), Pe’er & Ryde (2011), and others. In the fireshell model, which assumes an explosive energy release, the first potentially visible component of any GRB, the Proper GRB (Bianco et al. 2001; Ruffini et al. 2001), comes from the thermal flash of radiation emitted when the outflow becomes transparent for photons.

One of the main scopes of this paper is to show that the association of “instantaneous energy release” with “thin shell” (e.g. Piran et al. (1993) and Mészáros et al. (1993)) and “continuous energy release” with “thick wind” (e.g. Paczynski (1986, 1990)) generally adopted in the literature is incomplete with respect to the photospheric emission. A unified treatment of ultrarelativistic outflows originating both from instantaneous and from continuous energy release is presented here. We also propose a new classification of such outflows which is complementary to the traditional division on shells and winds. When photospheric emission is considered this new classification provides some additional physical insights. Based on these results we present a semi-analytic treatment for observed flux of photospheric emission assuming isotropic thermal distribution of scattered photons in the comoving frame. We compute both instantaneous and time-integrated spectra. These results are then applied within both the shell and the wind models of GRBs. Remarkably the time-integrated spectrum of energetic GRBs is predicted to have a Band shape (Band et al. 1993).

The structure of the paper is as follows. In Section 2 we discuss, compare and contrast an impulsive explosion and gradual energy release, giving rise respectively to an ultrarelativistic shell and wind. In Section 3 we present the computation of the optical depth and photospheric radius of the relativistic outflow and discuss applicability of recovered asymptotics to GRBs. In Section 4 we discuss radiation diffusion in an expanding relativistic outflow. Observed light curves and spectra of photon thick and photon thin outflows are computed in Sections 5 and 6, respectively. In Section 7 we discuss main results obtained in this work and their implications for GRBs. Conclusions follow. Details of derivation and application of the radiative diffusion approximation are given in Appendix.

2. OPTICALLY THICK RELATIVISTIC OUTFLOWS: WIND VS. EXPLOSION

Relativistic outflows are generally classified as *winds* or *shells* depending on how fast the energy in their sources is released. Consider energy release in a source of linear dimension R_0 . If the time scale of energy release is short $\Delta t \simeq R_0/c$, an explosion occurs, which may be characterized by the size R_0 , total energy released E_0 and total baryonic mass M . Relativistically expanding material forms a shell having width approximately R_0 . When the energy is released gradually, on a time scale $\Delta t \gg R_0/c$, but the source luminosity L exceeds the Eddington limit, a wind is formed, which is characterized by its activity time Δt , luminosity L and mass ejection rate \dot{M} .

In both wind and shell models of cosmological GRBs the region of energy release R_0 is clearly macroscopic, being of the order of the size of compact astrophysical objects, about $R_0 \sim 10^8$ cm. Considering the isotropic energy involved $E_0 \sim 10^{54}$ erg the temperature of plasma in this region is typically in MeV range. The time scale of thermalization in such plasma is of the order of 10^{-12} sec (Aksenov et al. 2007, 2010), being much shorter than the dynamical time scale R_0/c . Since such dense plasma is optically thick thermal equilibrium is established prior to expansion in both shell and wind models. Opacity in such plasma is dominated by Compton scattering. When the temperature in the source of the relativistic outflow is large enough for electron-positron pair creation, e^+e^- pairs make an additional contribution to the opacity.

Whether the outflow becomes relativistic or not depends on the entropy in the region where the energy is released. Both the wind and explosion cases can be parameterized (Shemi & Piran 1990) by a dimensionless entropy parameter η , equal to E_0/Mc^2 for shell model and $L/\dot{M}c^2$ for wind model. When the baryonic loading $B = \eta^{-1}$ (Ruffini et al. 2000) is sufficiently small the baryons will be accelerated to a relativistic velocity v of bulk motion, attaining large Lorentz factors up to $\Gamma = [1 - (v/c)^2]^{-1/2} \simeq \eta$, while in the opposite case of large baryonic loading the outflow remains nonrelativistic with $v \simeq c/\sqrt{2\eta}$.

In what follows we consider only ultrarelativistic spherically symmetric outflows with $\Gamma \gg 1$. In the simplest cases of wind or explosion in vacuum, the dynamics of the outflow is divided into an acceleration phase and a coasting phase (Piran 1999) with respectively

$$\Gamma \simeq \frac{r}{R_0}, \quad n_c \simeq n_0 \left(\frac{r}{R_0} \right)^{-3}, \quad R_0 < r < \eta R_0, \quad (1)$$

$$\Gamma \simeq \eta = \text{const}, \quad n_c \simeq \frac{n_0}{\eta} \left(\frac{r}{R_0} \right)^{-2}, \quad r > \eta R_0, \quad (2)$$

where n_c is the comoving number density of baryons in the outflow¹. Notice that in the case of an impulsive explosion for $r \gg R_0$ the matter and energy appear to a distant observer to be concentrated in a *geometrically thin* shell having width $l \sim R_0$ due to the relativistic contraction (Piran et al. 1993).

It is important to stress that both *an infinitely long wind* with a time-independent mass ejection rate and luminosity on the one hand, and *an infinitely thin shell* originating from an instantaneous explosion in infinitely thin region represent two limiting cases for the energy release.

During both acceleration and coasting phases the continuity

¹ All quantities with subscript "c" are measured in comoving reference frame, and all quantities without this subscript are measured in laboratory reference frame.

equation for the laboratory number density reduces to $n \propto r^{-2}$. We take for the laboratory density profile

$$n = \begin{cases} n_0 \left(\frac{R_0}{r} \right)^2, & R(t) < r < R(t) + l, \\ 0, & \text{otherwise,} \end{cases} \quad (3)$$

where $R(t)$ is the radial position of the inner boundary of the outflow. Such an outflow may be produced by a gradual energy release with constant luminosity and mass ejection rate on a finite time Δt and we will refer to it as the *portion of wind*.

Below we show that both the shell and the wind defined above may appear for photons emitted inside it as long wind or as thin shell, depending on the initial conditions that specify respectively their width l and activity duration Δt . This appearance is a consequence of ultrarelativistic expansion of the outflow. It is crucial to keep in mind that photons emitted inside the expanding outflow propagate in a medium whose laboratory number density depends both on radial coordinate and on time $n(r, t)$. For photons propagating in the wind the spatial dependence of the number density plays the key role, while for photons propagating in the shell its time dependence is crucial.

3. OPTICAL DEPTH AND PHOTOSPHERIC RADIUS

The optical depth along the photon world line \mathcal{L} is defined as

$$\tau = \int_{\mathcal{L}} \sigma j_{\mu} dx^{\mu}, \quad (4)$$

where σ is Thomson cross section, j^{μ} is the 4-current of particles, on which the photon scatters, and dx^{μ} is the element of the photon world line.

Consider a spherically symmetric expanding outflow with an ultrarelativistic velocity $v = \beta c \simeq 1 - 1/2\Gamma^2$. Assume that the photon is emitted at time t from the interior boundary $r = R$ of the outflow and it propagates outwards. This assumption is relaxed in Section 5.1. The optical depth computed along the photon path from (4) is (see e.g. Abramowicz et al. (1991))

$$\tau = \int_R^{R+\Delta R} \sigma n (1 - \beta \cos\theta) \frac{dr}{\cos\theta}, \quad (5)$$

where $R + \Delta R$ is the radial coordinate at which the photon leaves the outflow, and θ is the angle between the velocity vector of the outflow and the direction of propagation of the photon, n is the laboratory number density of electrons and positrons, which may be present due to pair production. Geometry of the outflow and used variables are illustrated by Fig. 1.

A pure electron-positron plasma reaches thermal equilibrium before expansion (Aksenov et al. 2007, 2010) and it remains accelerating until it becomes transparent to radiation. Due to exponential dependence of thermal pair density on the radial coordinate transparency is reached at

$$kT_{\pm} \simeq 0.040 m_e c^2 \quad (6)$$

rather independent of the initial conditions. Note that the optical depth for an expanding electron-positron-photon shell computed by Shemi & Piran (1990) is incorrect since it uses photon thin asymptotics, see 3rd line in (7) below, which never applies to the pure e^+e^- outflows. The formula (6) is

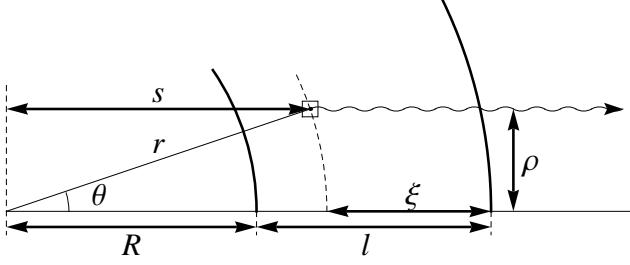


FIG. 1.— Geometry of the outflow and variables used. Observer is located to the right at infinity.

in agreement with works of Grimsrud & Wasserman (1998) and Li & Sari (2008).

Electron-positron plasma with baryonic loading also reaches thermal equilibrium before its expansion starts (Aksenov et al. 2009, 2010). With decreasing entropy η opacity due to electrons associated with baryons increases and eventually dominates over pair opacity. Straightforward calculations with the laboratory density profile (3) gives

$$\tau = \begin{cases} \frac{1}{6}\tau_0 \left(\frac{R_0}{R}\right)^3, & R_0 \ll R \ll \eta R_0, \\ \frac{1}{2\eta^2}\tau_0 \left(\frac{R_0}{R}\right), & \eta R_0 \ll R \ll \eta^2 l, \\ \tau_0 \frac{R_0 l}{R^2}, & R \gg \eta^2 l, \end{cases} \quad (7)$$

where

$$\tau_0 = \sigma n_0 R_0 = \frac{\sigma E_0}{4\pi m_p c^2 R_0 l \eta} = \frac{\sigma L}{4\pi m_p c^3 R_0 \eta}. \quad (8)$$

Let us interpret the formula (7). On the one hand, first two lines in (7) correspond to the case when the photon propagates inside the outflow for a significant time so that the number density on its path substantially decreases before it leaves. In this respect the outflow is “a long wind”, even if the laboratory thickness of the outflow may be small, $l \ll R$. We refer to this case as a *photon thick outflow*. On the other hand, the third line in (7) corresponds to the case when the number density of the outflow does not change substantially on the photon world line before it escapes. In this respect the outflow is “a thin shell” even if the duration of explosion could be long and a wind was launched. We refer to this latter case as a *photon thin outflow*. For instance, a geometrically thin ultrarelativistically expanding shell may be both thin or thick with respect to the photon propagating inside it.

Similar consideration may be applied to a photon emitted at any distance ξ from the outer boundary of the outflow, see Section 5.1. It is clear then, that even in a photon thick outflow there is always a photon thin layer located near the outer boundary. During acceleration phase such a photon thin part accounts for a fraction not larger than Γ^{-1} of the entire width of the outflow².

In the derivation of (7) we considered a portion of a relativistic wind, but these results are generic and apply to any density profile of the outflow.

² Formally photon thin accelerating solution exists, and it is given by the last line in (7). However, its validity condition is $l \ll R_0^2/R = R_0/\Gamma$.

The *photospheric radius* R_{ph} is defined by equating (7) to unity. It is worth noting that it is the lower limit in the integral (5) that is associated with the photospheric radius, but not the upper one. The upper limit in (5) is the radius at which the photon leaves the outflow, even if it may decouple from the outflow at much smaller radius, as in the photon thick case. The characteristic parameter which determines the type of the outflow at the photospheric radius is the ratio $\tau_0/(4\Gamma^4)$. When it is much smaller than one the outflow is photon thick, while in the opposite case the outflow is photon thin.

Consider now the shell model of GRBs with typical parameters expressing their total energy as $E_0 = 10^{54} E_{54}$ erg, initial size as $R_0 = l = 10^8 R_8$ cm and entropy parameter as $\eta = 10^2 \eta_2$. We find the following asymptotic solutions for the photospheric radius together with domains of their applicability

$$R_{ph} = \begin{cases} 4.4 \times 10^{10} (E_{54} R_8)^{1/4} \text{ cm}, \\ E_{54} \ll 4.8 \times 10^{-20} \eta_2^4 R_8^{-1}, \\ \hline 1.8 \times 10^{12} (E_{54} \eta_2^{-1} R_8)^{1/3} \text{ cm}, \\ 4.8 \times 10^{-20} \eta_2^4 R_8^{-1} \ll E_{54} \ll 3.2 \times 10^{-8} \eta_2^4 R_8^2, \\ \hline 1.8 \times 10^{17} E_{54} \eta_2^{-3} R_8^{-1} \text{ cm}, \\ 3.2 \times 10^{-8} \eta_2^4 R_8^2 \ll E_{54} \ll 1.1 \times 10^{-5} \eta_2^5 R_8^2, \\ \hline 5.9 \times 10^{14} (E_{54} \eta_2^{-1})^{1/2} \text{ cm}, \\ E_{54} \gg 1.1 \times 10^{-5} \eta_2^5 R_8^2. \end{cases} \quad (9)$$

For very small baryonic loading, or in other words for a pure electron-positron plasma, the photospheric radius does not depend on η parameter. For increasing baryonic loading it increases as $\eta^{-1/3}$ (accelerating photon thick solution). In both these cases the Lorentz factor at the photosphere is not equal to η , but it is much smaller. For larger baryonic loading the photospheric radius steeply increases as η^{-3} (coasting photon thick solution), and finally it increases as $\eta^{-1/2}$ (coasting photon thin solution), see Fig. 2. There we also show as function of the entropy parameter the following quantities computed at the photospheric radius: the Lorentz factor, the observed and comoving temperatures, and fraction of energy emitted from the photosphere to the total energy, for different values of the total energy E_0 . Dependence of parameters of transparency on initial conditions is also illustrated in Tab. 1. It is clear that the highest Lorentz factors at photospheric radius are attained in photon thick asymptotics. The largest transparency radii are reached instead in photon thin asymptotics.

Fig. 3 shows the energy-baryonic loading diagram, where the regions of validity of the asymptotics discussed above are indicated explicitly for typical parameters of GRBs. For all the relevant range of GRBs parameters $10^{48} \text{ erg} < E_0 < 10^{55} \text{ erg}$ and $10^6 \text{ cm} < R_0 < 10^{12} \text{ cm}$ all four asymptotics are present in the interval $10 < \eta < 10^{10}$.

TABLE 1
DEPENDENCIES OF TRANSPARENCY PARAMETERS ON INITIAL CONDITIONS: ENERGY E_0 , ENTROPY η , AND RADIUS R_0 FOR THE SHELL MODEL.

Regime of transparency	R_{ph}		Γ_{ph}		kT_{ph}			kT_{obs}	
Pair	$E_0^{1/4}$	$R_0^{1/4}$	$E_0^{1/4}$	$R_0^{-3/4}$	0.040 $m_e c^2$			$E_0^{1/4}$	$R_0^{-3/4}$
Acceleration	$E_0^{1/3}$	$\eta^{-1/3}$	$E_0^{1/3}$	$\eta^{-1/3}$	$E_0^{-1/12}$	$\eta^{1/3}$	$R_0^{-1/12}$	$E_0^{1/4}$	$R_0^{-3/4}$
Coasting photon thick	E_0	η^{-3}	E_0	η	$E_0^{-5/12}$	$\eta^{5/3}$	$R_0^{7/12}$	$E_0^{-5/12}$	$\eta^{8/3}$
Coasting photon thin	$E_0^{1/2}$	$\eta^{-1/2}$		η	$E_0^{-1/12}$		$R_0^{-1/12}$	$E_0^{-1/12}$	η

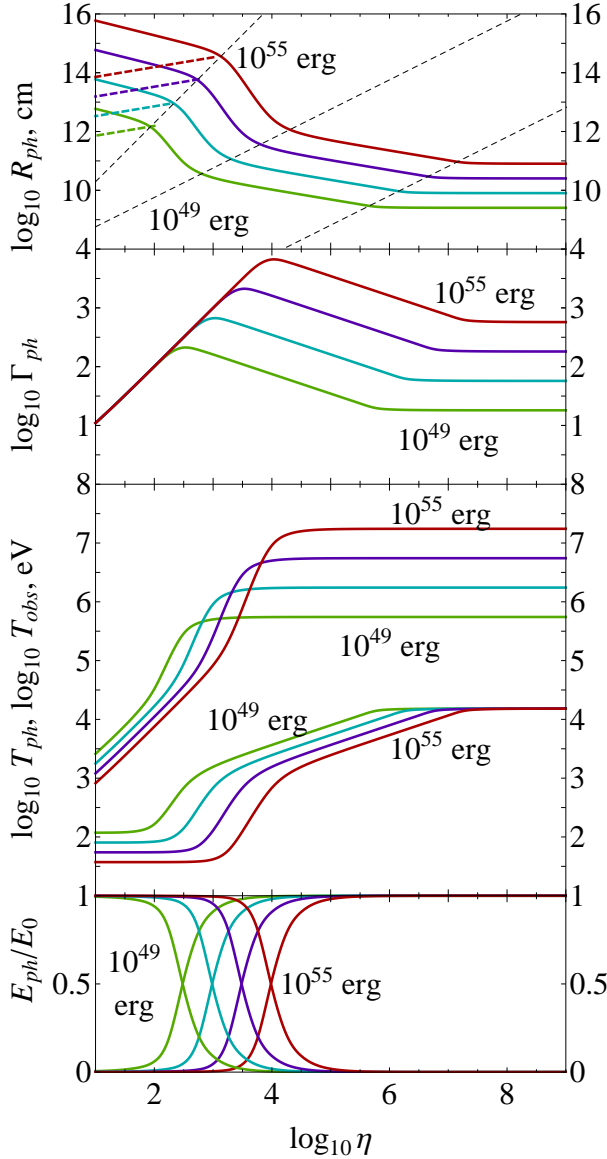


FIG. 2.— From top to bottom: photospheric radius R_{ph} , Lorentz factor Γ_{ph} , observed T_{obs} and comoving T_{ph} temperatures, and ratio of the energy emitted to the total energy E_{ph}/E_0 at photospheric radius as functions of entropy η for shells with different total energy E_0 but the same width $l = R_0 = 10^8$ cm. All four regimes with different asymptotics are clearly visible and dashed black lines corresponding to their domain of validity from Eq. (9) are shown. Curves are drawn for E_0 equal to: 10^{49} erg (green), 10^{51} erg (blue), 10^{53} erg (violet), and 10^{55} erg (red). Dashed thick lines denote the diffusion radius for each energy.

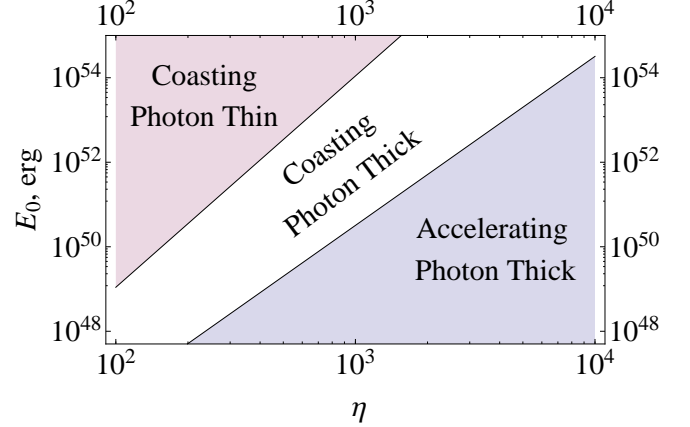


FIG. 3.— The energy-baryonic loading diagram showing the validity of the various asymptotic solutions for the photospheric radius for typical parameters of GRBs with $l = R_0 = 10^8$ cm.

In the case of gradual energy release resulting in relativistic wind an additional parameter is present, that is the duration of energy release, which we parameterize as $\Delta t = 1 \Delta t_1$ s. Instead of the total energy E_0 the luminosity $L = 10^{50} L_{50}$ erg/s is used. The corresponding photospheric radius is

$$R_{ph} = \begin{cases} 8.1 \times 10^8 L_{50}^{1/4} R_8^{1/2} \text{ cm,} \\ \quad L_{50} \ll 5.3 \times 10^{-15} \eta_2^4 R_8^{-2}, \\ \hline 1.3 \times 10^{10} (L_{50} \eta_2^{-1} R_8^2)^{1/3} \text{ cm,} \\ 5.3 \times 10^{-15} \eta_2^4 R_8^{-2} \ll L_{50} \ll 9.8 \times 10^{-2} \eta_2^4 R_8, \\ \hline 5.9 \times 10^{10} L_{50} \eta_2^{-3} \text{ cm,} \\ \quad 9.8 \times 10^{-2} \eta_2^4 R_8 \ll L_{50} \ll 10^5 \eta_2^5 \Delta t_1, \\ \hline 5.9 \times 10^{10} (L_{50} \Delta t_1 \eta_2^{-1})^{1/2} \text{ cm,} \\ \quad L_{50} \gg 10^5 \eta_2^5 \Delta t_1. \end{cases} \quad (10)$$

In Fig. 4 we show as function of the entropy parameter the following quantities computed at the photospheric radius: the Lorentz factor, the observed and comoving temperatures, and fraction of energy emitted from the photosphere to the total energy, for different duration of the wind with the total energy $E_0 = 10^{51}$ erg, and inner boundary radius $R_0 = 10^8$ cm. Wind duration ranges from 10 ms to 10 s. The correspond-

TABLE 2
DEPENDENCIES OF TRANSPARENCY PARAMETERS ON INITIAL CONDITIONS: ENERGY RELEASE RATE L , ENTROPY η , DURATION Δt , AND RADIUS R_0 FOR THE WIND MODEL.

Regime of transparency	R_{ph}			Γ_{ph}			kT_{ph}			kT_{obs}			
Pair	$L^{1/4}$	$R_0^{1/2}$		$L^{1/4}$	$R_0^{-1/2}$		$0.040m_e c^2$			$L^{1/4}$	$R_0^{-1/2}$		
Acceleration	$L^{1/3}$	$\eta^{-1/3}$	$R_0^{2/3}$	$L^{1/3}$	$\eta^{-1/3}$	$R_0^{-1/3}$	$L^{-1/12}$	$\eta^{1/3}$	$R_0^{-1/6}$	$L^{1/4}$		$R_0^{-1/2}$	
Coasting photon thick	L	η^{-3}		η			$L^{-5/12}$	$\eta^{5/3}$	$R_0^{1/6}$	$L^{-5/12}$	$\eta^{8/3}$	$R_0^{1/6}$	
Coasting photon thin	$L^{1/2}$	$\eta^{-1/2}$	$\Delta t^{1/2}$	η			$L^{-1/12}$	$\Delta t^{-1/3}$	$R_0^{1/6}$	$L^{-1/12}$	η	$\Delta t^{-1/3}$	$R_0^{1/6}$

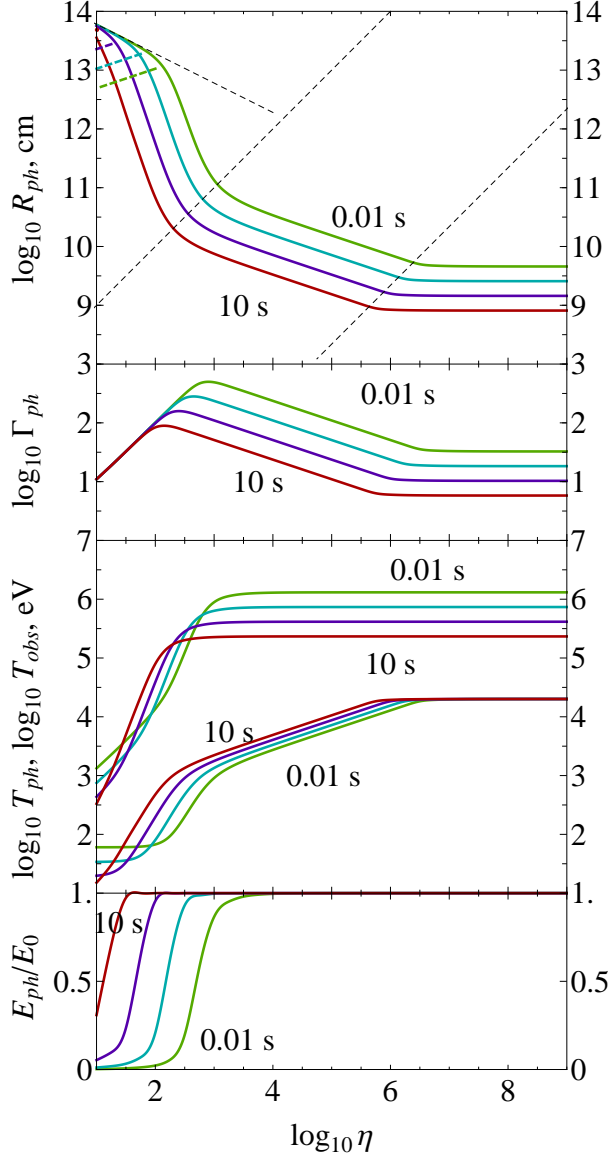


FIG. 4.— The same as in Fig. 2 for winds with different duration, but the same total energy $E_0 = 10^{51}$ erg and radius of origin $R_0 = 10^8$ cm. All four regimes with different asymptotics are clearly visible. Curves are drawn for Δt ranging from 10^{-2} s (green) to 10 s (red) in steps of one order of magnitude.

ing wind luminosity varies from 10^{53} erg/s to 10^{50} erg/s. Fig. 5 shows the luminosity-baryonic loading diagram where the regions of validity of the asymptotics discussed above are indicated. Dependence of transparency parameters on the initial conditions of the wind is presented in Tab. 2.

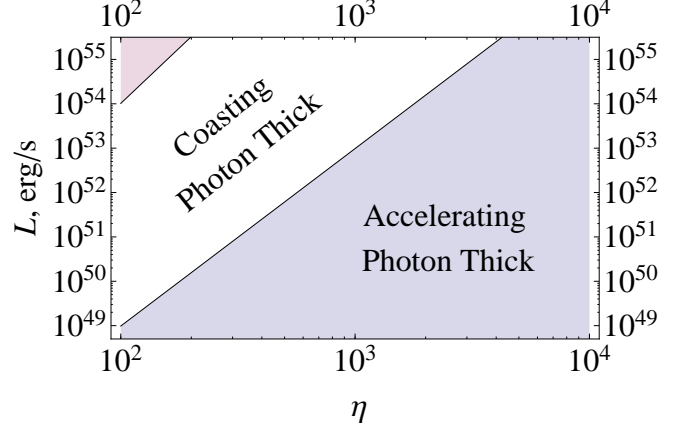


FIG. 5.— The luminosity-baryonic loading diagram showing the validity of the various asymptotic solutions for photospheric radius of wind with duration $\Delta t = 0.1$ s. Notation is the same as on Fig. 3.

3.1. Comparison with previous works

The expressions for the optical depth of a relativistic wind were obtained e.g. by Mészáros & Rees (2000). Their formulas coincide with our (7) up to a numerical factor which comes from the integration over the radial coordinate. It should be noted, however, that only the photon thick asymptotic limit is discussed in Mészáros & Rees (2000). The photon thin asymptotic limit may also be valid for relativistic winds in the coasting phase, provided that $l \ll R/(2\eta^2)$. This is an independent condition from $\Delta t \gg R_0/c$ and it is therefore possible to give the following constraints for Δt under which the outflow takes the form of a wind, but it is photon thin at the photospheric radius:

$$\frac{R_0}{c} \ll \Delta t \ll \frac{\tau_0 R_0}{4\eta^4 c}. \quad (11)$$

photospheric radius for photon thick and photon thin asymptotics for a portion of the coasting relativistic wind was obtained by Daigne & Mochkovitch (2002).

Similar considerations apply to an ultrarelativistic shell which is considered e.g. in Shemi & Piran (1990) and Mészáros et al. (1993) and by Ruffini et al. (2000) in the photon thin approximation. The corresponding condition that the shell at the photospheric radius appears to be photon thin is $\tau_0 \gg 4\eta^4$. It is possible, however, that initial conditions satisfy the opposite constraint which results in a photon thick shell, see Nakar et al. (2005).

Numerical hydrodynamic simulations produce complex density, temperature and Lorentz factor profiles of the outflow. In particular, Piran et al. (1993) and Mészáros et al. (1993) considered an explosion in a compact region with radius R_0 and studied numerically the hydrodynamic evolution of an optically thick plasma with various initial conditions.

They have shown that the plasma forms a relativistically expanding shell with some density and velocity profiles. The characteristic width of the density profile appears to be constant up to large radii, but later it increases linearly with radius due to the fact that the Lorentz factor appears to be monotonically increasing within the main part of the profile

$$l \simeq R_0, \quad R < \eta^2 R_0, \quad (12)$$

$$l \propto R, \quad R > \eta^2 R_0. \quad (13)$$

Such a spreading in density profile may result in a substantial increase in the width $l \gg R_0$ of the shell when it becomes transparent to radiation. Note that condition (13) coincides with the condition in the third line of (7), which corresponds to the case of a photon thin outflow. This coincidence may give an impression that photon thin asymptotics does not exist for hydrodynamically spreading outflows. Nevertheless direct integration of (5) in numerical simulations shows that the photon thin asymptotics is valid even for the shell undergoing such spreading.

All asymptotic solutions for the optical depth have been considered by Mészáros et al. (2002), except the case of pure electron-positron outflow. They derived the photospheric radius considering the expansion in comoving reference frame. Notice, that the photon thin asymptotics is obtained in Mészáros et al. (2002) by assuming hydrodynamic spreading of the outflow found by the same authors in (Mészáros et al. 1993). In absence of such spreading (e.g. portion of wind considered above) such asymptotics cannot be obtained this way. Finally, Toma et al. (2011) discuss all asymptotic solutions, applying them to a relativistic wind.

We conclude that interpretation of the formula (7) in terms of photon thick and photon thin conditions given above provides additional physical insight to the consideration of optical depth in shell and wind models.

4. PHOTON DIFFUSION

Up to now we assumed that photons escape the expanding outflow when its optical depth decreases to unity. We have distinguished two possibilities:

- in the photon thick case electron number density decreases along the photon path so rapidly that the medium becomes too rarified to sustain collisions. Most photons however still remain inside the outflow after decoupling;
- in the photon thin case the variation of the electron number density along the photon path can be neglected, but the mean free path of photons increases with expansion and eventually exceeds the radial thickness of the outflow.

In all the previous discussion we explicitly neglected the effect of radiative diffusion out of the outflow by random walks of photons. Diffusion time is given by $t_{D,c} = l_c^2/D_c$, where $l_c = \Gamma l$ is the comoving radial thickness of the outflow, and diffusion coefficient is $D_c = (c\lambda_c)/3 = c/(3\sigma n_c)$, where λ_c and n_c are comoving mean free path of photons and comoving electron number density, respectively.

In order to determine at which radii diffusion becomes important one has to compare this diffusion time with comoving expansion time of the outflow $t_c = R/(c\Gamma)$. Taking into account (3) and (8) we obtain that it happens when the outflow

reaches the radius

$$R_D = (\tau_0 \eta^2 R_0 l^2)^{1/3} \simeq \begin{cases} 7.2 \times 10^{13} (E_{54} l_8 \eta_2)^{1/3} \text{ cm}, \\ 5.0 \times 10^{11} (L_{50} \Delta t_1^2 \eta_2)^{1/3} \text{ cm}. \end{cases} \quad (14)$$

This diffusion radius turns out to be always larger than the photospheric radius of photon thick outflows, $R_D \gg R_{ph}$, so that diffusion is irrelevant for their description. In the opposite case of photon thin outflows instead the diffusion radius is always smaller than the photospheric radius $R_D \ll R_{ph}$. In this case most radiation leaves the photon thin outflow not at its photospheric radius, but before it reaches the diffusion radius, when the outflow is still opaque. In other words, the decoupling of photons from the outflow occurs not locally, as in the photon thick case, but near its boundaries where photons are transferred to by diffusion. In this sense the characteristic radius of the photospheric emission is not the photospheric radius found from (7), but the radius of diffusion (14). Besides, the comoving temperature of escaping radiation is different from that discussed in Section 3.

In what follows we consider decoupling of photons from photon thick and photon thin outflows separately.

5. PHOTOSPHERIC EMISSION FROM PHOTON THICK OUTFLOWS

5.1. Geometry and dynamics of the photosphere

Unlike traditional static sources usually dealt with in astrophysics, relativistic outflows may have strongly time-varying photospheres. For the portion of wind the optical depth can be calculated analytically both at acceleration and coasting phases for photon thin and photon thick outflows. The result is

$$\begin{aligned} \tau(r, \theta, t) = \tau_0 R_0 \left\{ \frac{1}{r \sin \theta} \left[\theta - \tan^{-1} \left(\frac{r \sin \theta}{cT + r \cos \theta} \right) \right] \right. \\ \left. - \beta_m \left(\frac{1}{r} - \frac{1}{\sqrt{(cT + r \cos \theta)^2 + (r \sin \theta)^2}} \right) \right. \\ \left. + \frac{R_0^2}{6} \left(\frac{1}{r^3} - \frac{1}{[(cT + r \cos \theta)^2 + (r \sin \theta)^2]^{3/2}} \right) \right\}, \quad (15) \end{aligned}$$

where T is the time interval during which photon remains inside the outflow, determined by the equations of motion of the photon and of the outflow, and $\beta_m = 1 - 1/(2\eta^2)$. For a given laboratory time t the photosphere geometry $r = r(\theta)$ is obtained by equating (15) to unity. Then formula (15) gives complete information on the dynamics and geometry of the photosphere of portion of ultrarelativistic wind. In order to understand this dynamics it is instructive to consider its limiting cases.

Firstly, the photosphere of the coasting infinitely long relativistic wind with $\Gamma = \text{const}$ analyzed by Abramowicz et al. (1991) may be recovered from (15) with $T \rightarrow \infty$. In that case the last term in (15) can be neglected and we have (see e.g. Pe'er (2008))

$$\frac{r}{R_0} = \tau_0 \left(\frac{\theta}{\sin \theta} - \beta_m \right), \quad (16)$$

which is a static surface having concave shape, see Fig. 6.

Secondly, the photosphere of the accelerating infinite wind may be obtained from (15) for $T \rightarrow \infty$ and $\eta \rightarrow \infty$. It results in a cubic equation describing a static surface with curvature

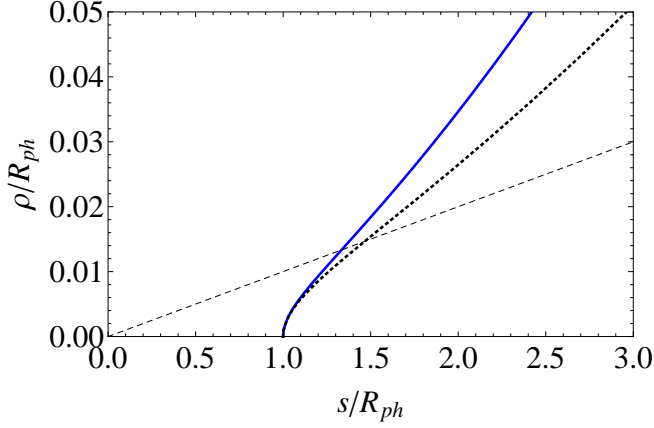


FIG. 6.— The shape of photospheres of infinitely long coasting (blue solid curve) and accelerating (black dotted curve) winds for $\Gamma_{ph} = 100$. Dashed line shows the relativistic beaming angle.

larger than that of the coasting wind, see Fig. 6. In both cases these photospheres appear for a distant observer as static spots with radius

$$\rho = \pi\tau_0 R_0 \quad (17)$$

and brightness decreasing from the center to the edge.

Now consider dynamic properties of the photosphere of photon thick outflow described by (15) as seen by a distant observer. The arrival time of radiation is defined as $t_a = t - r \cos \theta / c$. The equitemporal surface (EQTS) of the photospheric emission represents a part of the photosphere visible at a given instant of arrival time t_a , see e.g. Ruffini et al. (2001). We will refer to that surface as *Photospheric EQTS* (PhE).

PhE of the photon thick outflow has concave shape, see Fig. 7 and Fig. 8 for accelerating and coasting cases, respectively. This concave PhE in both cases approaches the photosphere of infinitely long wind. In the coasting case the approach to that surface is only asymptotic, while in the accelerating case the photosphere actually reaches it at finite arrival time. The external boundary of the PhE for a given t_a shown in Fig. 8 is defined by the condition that the optical depth for photons emitted from the outermost layer of the outflow equals unity. Notice that this boundary is wider than the relativistic beaming surface (these are tube and cone for accelerating and coasting outflows, respectively). As soon as the innermost part of the outflow reaches the photospheric radius, i.e. observer sees the switching off of the wind, the inner boundary of the PhE expands with t_a . The surface of these boundaries is given by (16) in the case of coasting photon thick outflow.

5.2. Observed flux and spectrum

The basis of spectrum and flux calculation is radiative transfer equation for specific intensity I_ν along the ray (see e.g. Rybicki & Lightman (1979), p. 11)

$$\frac{dI_\nu}{ds} = j_\nu - \kappa_\nu I_\nu, \quad (18)$$

where j_ν is monochromatic emission coefficient, κ_ν is absorption coefficient and s is distance, measured along the ray.

Spectral intensity of radiation at infinity on a ray coming to observer at some arrival time t_a is given by formal solution of

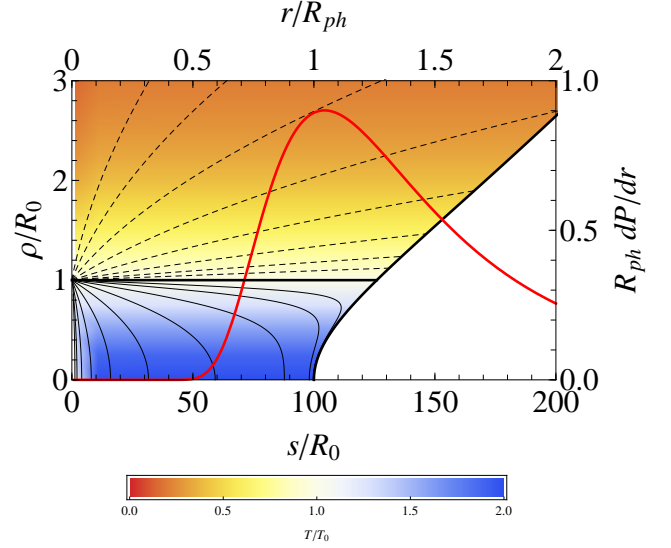


FIG. 7.— PhE of the photon thick accelerating outflow at different arrival times, and the probability density function of photon last scattering integrated over angles $P(r)$ (red thick curve). Thick black curve represents the photosphere of infinitely long accelerating wind. PhEs are illustrated for several arrival times with logarithmic spacing by thin black curves. The surface $\cos \theta = \beta$ is given by $\rho = R_0$ and it is shown by thick black line. Dashed curves illustrate the maximal visible size ρ for several arrival times with logarithmic spacing. The PhE at that arrival times is a part of the wind photosphere limited by the corresponding curves. Range of observed temperature of emission under the asymptotic photosphere is illustrated by color, see legend. Here $R_{ph} = 100R_0$.

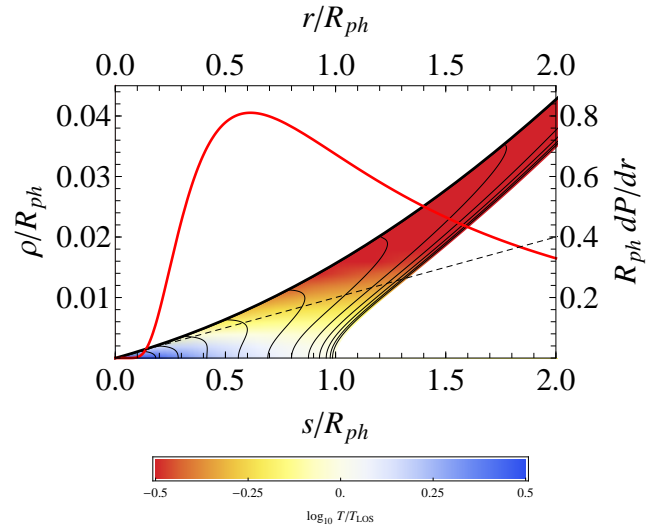


FIG. 8.— The same as in Fig. 7 for a photon thick coasting outflow. PhEs are illustrated by thin curves for several arrival times with linear spacing. Thick black curve bounding PhEs correspond to the position of maximal visible angles at given t_a . Notice that these angles exceed the relativistic beaming angle, shown by dashed black line. Right edge of the colored area is the photosphere of infinitely long coasting wind (16). Here $\Gamma = 100$.

this equation

$$\begin{aligned} I_\nu(\nu, \rho, t_a) &= \int \mathcal{I}_\nu(\nu, r, \theta, t) \frac{d}{ds} \{ \exp[-\tau(\nu, r, \theta, t)] \} ds \\ &= \int \mathcal{I}_\nu(\nu, r, \theta, t) \exp[-\tau(\nu, r, \theta, t)] d\tau, \end{aligned} \quad (19)$$

where $\mathcal{I}_\nu(r, \theta, t)$ is the source function, equal to the ratio

of emission and absorption coefficients $\mathcal{I}_\nu = j_\nu/\kappa_\nu$, optical depth τ is an integral of κ_ν from the point on the ray under consideration to infinity $\tau = \int \kappa_\nu ds$, and variables (r, θ, t) are connected by $t_a = t - r \cos \theta$ and $r \sin \theta = \rho$, see Fig. 1. We use Thomson scattering cross section in comoving frame $\kappa_c = \text{const}$.

Total observed flux is an integral over all rays

$$F_\nu(\nu, t_a) = 2\pi \Delta\Omega \int \rho d\rho I_\nu(\nu, \rho, t_a) \quad (20)$$

where $\Delta\Omega$ is the solid angle of the observer's detector as seen from the outflow in the laboratory frame and $2\pi\rho d\rho$ is an element of area in the plane of the sky.

In what follows we assume that emissivity j_ν is thermal and isotropic in comoving frame of the outflow. The laboratory source function is then

$$\mathcal{I}_\nu(\nu, r, \theta, t) = \frac{2h}{c^2} \frac{\nu^3}{\exp\left(\frac{h\nu\Gamma(1-\beta\cos\theta)}{kT_c(r,t)}\right) - 1}. \quad (21)$$

This approximation is justified when the radiation field is tightly coupled to the matter. The photospheric emission comes from entire volume of the outflow, and the computational method sketched above is closely related to that used in (Beloborodov 2011) where the concept of ‘‘fuzzy photosphere’’ was introduced. This method will be referred to as *fuzzy photosphere* approximation.

Most of energy reaching observer is emitted from the region near the PhE, where the probability density function along the ray

$$P(r, \theta, t) = P_0 \frac{d}{ds} \exp[-\tau(r, \theta, t)] \quad (22)$$

with P_0 being normalization, reaches the maximum. For this reason the dynamics of PhE studied in the previous section determines both light curves and spectra of observed photospheric emission. When the time dependence in this equation is discarded this $P(r, \theta)$ coincides with the probability density function of the last scattering defined in (Pe'er 2008). Assuming that all the energy comes from the PhE only, i.e. a surface instead of the volume discussed above, the computation may be reduced to one dimensional integration by substitution of the function P with a Dirac delta. Such more crude approximation, in contrast to the fuzzy photosphere one, will be referred to as *sharp photosphere* approximation.

For photon thick outflow the optical depth becomes function of r and θ only and the comoving temperature also depends only on radius. In this respect the photon thick case is similar to the infinite wind. Then the integrand in (20) does not depend on time and only limits of integration provide time dependence due to motion of the outflow boundaries. The probability density function (22) integrated over angles is shown in Figs. 7 and 8 for accelerating and coasting photon thick outflows.

The observed flux of photospheric emission from accelerating outflow is illustrated in Fig. 9 by thick red curve (fuzzy photosphere) and by dotted blue curve (sharp photosphere). The characteristic raising and decaying time is in both cases

$$\delta t = \frac{R_0^2}{(R_{ph}c)} = \frac{R_0}{\Gamma_{ph}c}. \quad (23)$$

There is no simple analytic expression describing full light curve, however its decreasing part is close to a power law with

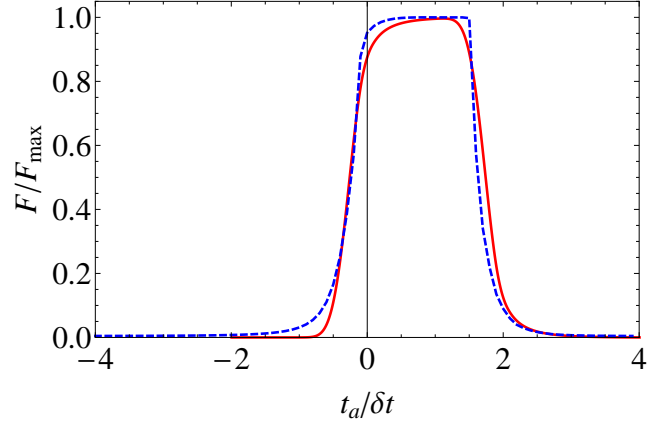


FIG. 9.— The light curve of photospheric emission from the photon thick accelerating outflow in fuzzy (red curve) and sharp photosphere approximations (dashed blue curve). Here $R_{ph} = 100R_0$, and $\Delta t = 2\delta t$, see (23) below.

index -4.7 and -6.5 within fuzzy and sharp photosphere approximations, respectively. As minimal duration of the photon thick outflow Δt is of order R_0/c , then $\Delta t \gg \delta t$ and the light curve has almost rectangular shape.

Such accelerating outflow appears to a distant observer as a spot with size $\rho = (R_0^2 - (t_a/c)^2)^{1/2}$, for $-R_0/c \leq t_a \leq 0$. As soon as the PhE reaches the corresponding accelerating infinitely long wind photosphere at $t_a = 0$ the spot size starts to increase almost linearly with time $\rho \simeq R_0 + ct_a$. Finally, as the innermost part of the outflow reaches the photospheric radius the spot transforms to a ring with rapidly decreasing width and brightness.

The observed photospheric emission of the coasting photon thick outflow results in the flux changing as

$$F = F_{max} [1 - (t_p/t_a)^2], \quad (24)$$

with

$$t_p = \frac{R_{ph}}{2\eta^2 c}, \quad (25)$$

i.e. increase up to the saturation value $F_{max} \propto L$, see the raising part of the light curve in Fig. 10, both in sharp and fuzzy photosphere approximations. Radius of the visible spot then reaches its maximal size (17). As arrival time exceeds $t_p + \Delta t$ the innermost part of the outflow approaches the wind photosphere (16) along the line of sight and the spot transforms to a ring, the flux decreases rapidly in both approximations

$$F \propto t_p^2 \left[\frac{1}{(t_a - \Delta t)^2} - \frac{1}{t_a^2} \right]. \quad (26)$$

For $t_a \gg \Delta t$ it behaves as $F \propto t_a^{-3}$, see the decreasing part of the light curve in Fig. 10. Similarly to the accelerating photon thick outflow the light curve for $\Delta t \gg t_p$ has almost rectangular shape due to the fact that its increase and decay times are much shorter than Δt .

Accelerating photon thick outflows exhibit photospheric spectra close to thermal ones, see Fig. 11. In ultrarelativistic case spectra computed using both sharp and fuzzy photosphere approximations are very close to each other. Both have small deviations from thermal spectrum in the low energy part with the corresponding Band low energy indices $\alpha = 0.82$ and $\alpha = 0.71$, respectively.

In contrast, the spectrum of photospheric emission of the coasting photon thick outflow is significantly wider than the

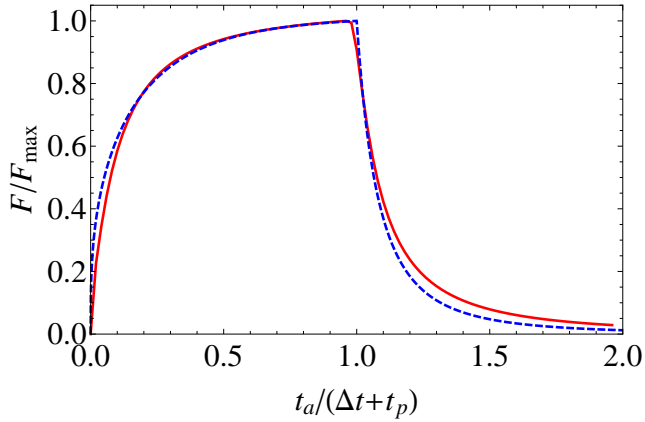


FIG. 10.— The same as in Fig. 9 for a photon thick coasting outflow. Here $\Gamma = 100$ and $\Delta t = 5t_p$, see (25) below.

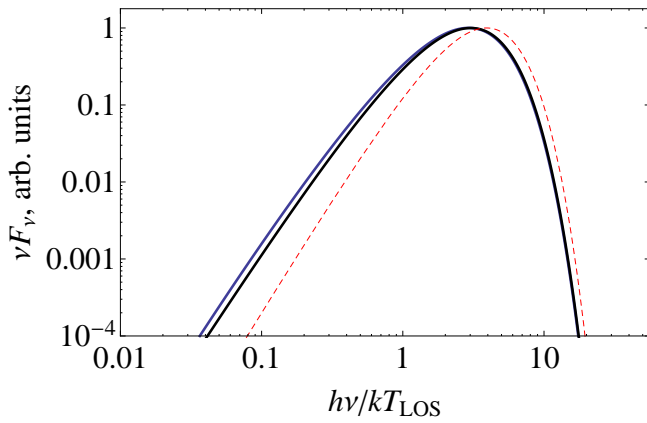


FIG. 11.— Instantaneous spectrum of photospheric emission of accelerating photon thick outflow in continuous (blue thick curve) and sharp photosphere approximation (black thick curve). Dashed red curve represents the thermal spectrum with the temperature at the line of sight T_{LOS} . Lorentz factor at photospheric radius is $\Gamma_{ph} = 100$.

thermal spectrum, see Fig. 12. Low energy part is described by a power law with Band indices respectively $\alpha = 0.34$ and $\alpha = 0$, for sharp and fuzzy photosphere approximations.

After initial phase of evolution, namely rising of the low-energy part, spectra do not evolve until observer detects emission from the innermost part of the outflow. At that moment there is a transition to another phase characterized by the fast decrease of both temperature and flux. Considering time-integrated spectrum we find that as characteristic times of the first and third phases are much less than that of the second one, the spectrum is close to the instantaneous one described above.

5.3. Comparison with previous works

Now we compare the results with obtained by other methods. Beloborodov (2011) considered the photospheric emission from infinitely long wind both at acceleration and coasting phases and solved the corresponding *steady* radiative transfer equation. His main conclusion is that in addition to usual relativistic beaming leading to anisotropy of radiation in laboratory frame, in the coasting wind another anisotropy in the comoving frame of the outflow is developing. This comoving anisotropy results from the fraction of photons which already underwent their last scattering in the bulk photon field

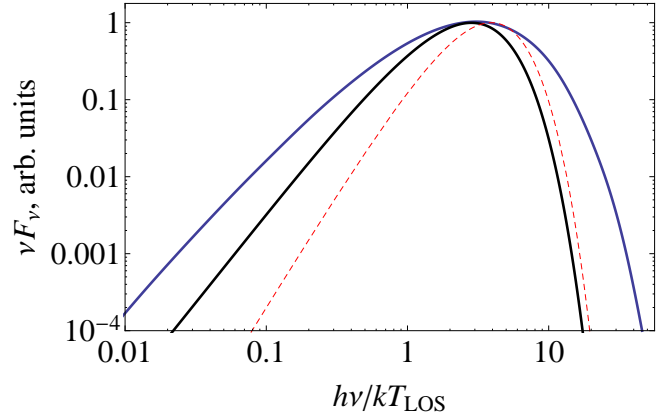


FIG. 12.— The same as in Fig. 9 for a photon thick coasting outflow with Lorentz factor $\Gamma = 100$.

of the outflow. The anisotropy of such photons grows with increasing radius for geometrical reasons. Since the amount of such photons increase with radius the entire photon field becomes increasingly anisotropic.

For the finite photon thick outflow the radiative transfer problem becomes explicitly time dependent. The expanding outflow at a given laboratory time spans only a finite part of the probability density distribution shown in Figs. 7 and 8, that results in difference in observed spectra for finite and infinite cases. Interesting consequence of ultrarelativistic motion of the outflow is that even geometrically thin outflow $l \ll R$ at a given arrival time spans large interval of laboratory radius $\Delta r = 2\Gamma^2 l$.

The effect of additional comoving anisotropy on the source function found by Beloborodov (2011) is actually small. The difference between the probability of last scattering (22) and the distribution of last scattering in a steady wind does not exceed several percent.

Our method is also similar to the one used by Pe'er (2008) and by Pe'er & Ryde (2011) who described the late-time photospheric emission of switching off relativistic wind considering the probability density function (22) for the last scattering of photons. An additional approximation adopted by these authors is the possibility to split radial and angular dependencies. Actually Pe'er (2008) computes not the traditional energy flux understood as energy crossing unit area in unit time, but photon flux as number of photons crossing unit area in unit time. For this reason his decay law for photon flux at late times is $F^{ob}(t_a) \propto t_a^{-2}$. Lorentz transformation of the photon energy from the comoving frame to the laboratory one results in additional multiplier $(1 - \beta\mu)^{-1}$ in the energy flux that leads to the observed flux $F \propto t_a^{-3}$, which agrees with our result in Eq. (26), see also Pe'er & Ryde (2011).

We conclude that the fuzzy photosphere approximation in fact follows closely methods of Pe'er & Ryde (2011) and Beloborodov (2011). In fact we obtained similar results for the probability of last scattering as more sophisticated treatment of radiation transfer (Beloborodov 2011). The sharp photosphere approximation provides good description of light curves including their raising and decaying parts. The observed spectrum from accelerating outflow is also well described in this approximation, while there is some difference for the coasting case. The advantage of sharp photosphere approximation for computing observed light curves and spectra

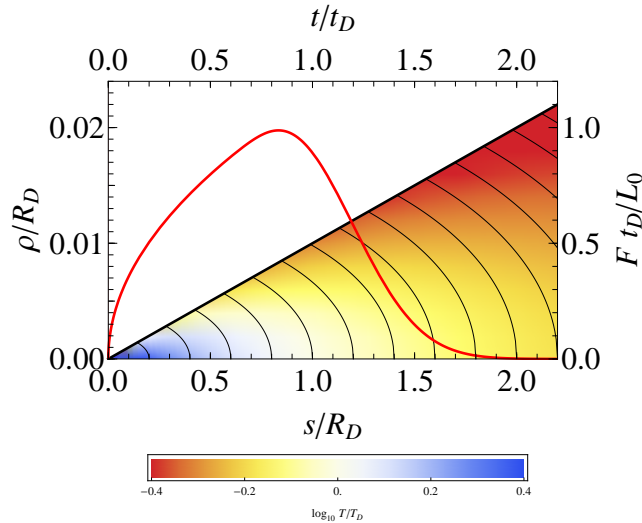


FIG. 13.— Evolution of PhE for the photon thin coasting outflow and dimensionless radiative diffusion flux, corrected for adiabatic cooling (red thick curve). PhEs shown by thin curves correspond from left to right to arrival times $t_a = (t_a^D/5, 2t_a^D/5, \dots)$, see (29). Thick black curve bounding PhEs correspond to the surface $\cos\theta = \beta$. Relevant range of observed temperature of photospheric emission is illustrated by color, see legend. Here $\Gamma = 100$.

is evident for intrinsically variable and dynamic outflows.

6. PHOTOSPHERIC EMISSION FROM PHOTON THIN OUTFLOWS

Now we turn to photon thin outflows. In Section 4 we pointed out that most of the radiation leaves the outflow not at its photospheric radius, but earlier, before the diffusion radius. Given that opacity of the outflow is still large, the emission escapes only from a very narrow region near the outer boundary of the outflow. The probability density function (22) is strongly peaked there and the photospheric emission for a given arrival time originates from this narrow region. Sharp photosphere approximation is thus completely justified in this case.

Since all the radiation is emitted from the PhE we briefly discuss its geometry and dynamics. The PhE of the photon thin outflow is similar to EQTS of infinitesimally thin constantly emitting relativistic shell considered firstly by Couderc (1939) and then by Rees (1966, 1967). The EQTS of this shell appears to a distant observer as an ellipsoid with axes ratio equal to Γ . However the PhE of photon thin outflow is not the entire ellipsoid: it is only a part of that surface, see Fig. 13. The external boundary of the PhE for a given t_a is defined by the condition that photons emitted from the outermost layer of the outflow toward observer leaves the outflow. In the photon thin asymptotics this surface coincides with the relativistic beaming cone.

We again start with the radiative transfer equation (18). In contrast with the photon thick case, here the source function \mathcal{I} in (19) strongly depends on both r and t . The main process by which photons are coupled to the matter is Compton scattering which conserves the number of photons. Since opacity is large other processes which do not conserve the photon number lead to local thermodynamic equilibrium with thermal comoving radiation intensity I_c , number density and spectrum of photons in the outflow. Hence we use the Rosseland radiative diffusion approximation (see e.g. Rybicki & Lightman (1979), pp. 39–42), that we derive from the radiative transfer

equations (18) for expanding outflows. Details of calculations are presented in Appendix.

It is useful to introduce the function $L_c(\xi, t) = (t/t_0)^{8/3} I_c(\xi, t)$ which accounts for the adiabatic cooling of radiation in expanding outflow. Here both ξ and time t are measured in laboratory frame, while $I_c(\xi, t)$ is measured in comoving frame. The diffusion equation with these variables is well behaved in ultrarelativistic limit, see Beloborodov (2011). We then obtain

$$\frac{\partial L_c}{\partial ct} - \frac{c^2 t^2 \Delta}{3R_0} \frac{\partial^2 L_c}{\partial \xi^2} = 0, \quad \Delta = \frac{1}{\Gamma^2 \tau_0}. \quad (27)$$

Notice that the diffusion coefficient is explicitly time dependent due to the expansion of the outflow. In Appendix we also discuss initial and boundary conditions and obtain an approximate analytic solution for the radiation field inside the photon thin outflow, which is represented in Fig. 13. The raising part of the corresponding flux of L_c through the external boundary of the outflow scales as $t^{1/2}$, while its decaying part is quasi-exponential one. Consequently, while the diffusion in a static object gives the flux decreases as $t^{-1/2}$, in our case the observed flux (20) is a more slowly decreasing function

$$F \propto t_a^{-1/6}, \quad (28)$$

up to arrival time of diffusion

$$t_a^D = \frac{R_D}{2\eta^2 c} \simeq 0.12 E_{54}^{1/3} \eta_2^{-5/3} l_8^{1/3} \text{ s}, \quad (29)$$

where large part of energy has left the outflow already. At this moment the energy decrease due to diffusion becomes substantial even in the deepest parts of the outflow and later the observed flux decreases quasi-exponentially with arrival time.

The comoving temperature of radiation on the photosphere is determined by the balance between the energy diffusion from the interior of the outflow and radiative losses and it is much smaller than the temperature in the interior. The variation of observed temperature across the PhE is small, see Fig. 13 and hence the observed instantaneous spectrum is very close to the thermal one and peaks near the observed temperature on the line of sight. We find that the latter decreases as $t_a^{-13/24}$, in contrast with adiabatic law $t_a^{-2/3}$. However, at diffusion radius both temperatures coincide giving for the line of sight temperature

$$T_{LOS} \simeq 162 \eta_2^{4/9} \text{ keV}. \quad (30)$$

The time integrated spectrum has a Band shape with a cut-off near the temperature of transition from acceleration to coasting, see Fig. 14. Low energy part of the spectrum has the slope $\alpha = 1$, while high-energy part has $\beta \simeq -3.5$.

7. DISCUSSION

The expression (29) gives an estimate for duration of photospheric emission of photon thin outflows. When available observed spectra are integrated on time intervals comparable to (29) the observed spectrum of photospheric emission is expected to have Band shape. Thus, starting from comoving thermal spectrum for the photospheric emission we obtain for the first time an observed spectrum which may be well described by the Band function with high energy power law index β being determined by the density profile of the outflow. We find this result quite remarkable.

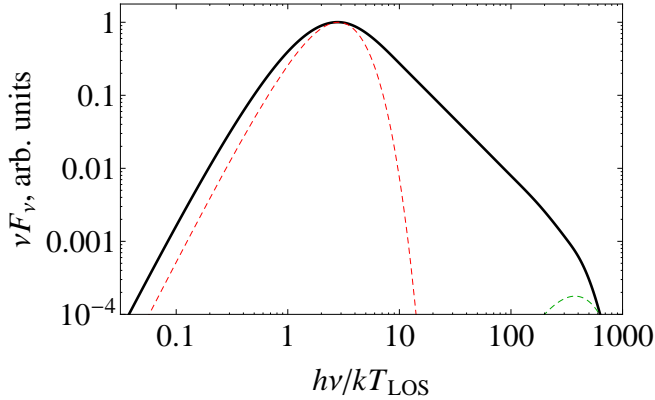


FIG. 14.— Time-integrated spectrum of photospheric emission of photon thin outflow (thick curve, $\eta = 100$, $R_D = 10^3 R_0$), superimposed with two instantaneous spectra of that emission, corresponding to arrival time of photons emitted at the moment of transition from acceleration to coasting (dashed green curve on the right) and to arrival time of diffusion (dashed red curve on the left).

Notice that non thermal spectra as a result of convolution of thermal ones over time has been introduced for afterglows of GRBs by Blinnikov et al. (1999). Double convolution over EQTS and arrival time is also one of the key ideas in the fireshell model (Ruffini et al. 2003).

Band spectra in photospheric models of GRBs have been obtained by now only assuming additional dissipation mechanisms such as magnetic reconnection (Giannios 2006), collisional heating (Beloborodov 2010) and internal shocks (Toma et al. 2011; Ryde et al. 2011b). In our model such additional assumption is not required.

It is even more remarkable that GRBs appear to be the only known objects in nature able to reach the photon thin asymptotics in their ultrarelativistic expansion. For thermally accelerated relativistic plasmas which are discussed in connection with their possible synthesis in ground based laboratories (e.g. Ruffini et al. (2010)) it is unreachable. The photon thin asymptotics is reached if the optical depth (8)

$$\tau_0 \gg 4\Gamma^4 \frac{l}{R_0} = 4 \times 10^8 \eta_2^4 \frac{l_8}{R_8}. \quad (31)$$

GRBs clearly can satisfy this constraint as the contribution of baryons $\tau_0 \simeq 3.5 \times 10^{13} E_{54} \eta_2^{-1} R_8^{-1} l_8^{-1}$.

We obtained both time integrated and instantaneous observed spectra of accelerating photon thick outflow which are close to thermal one with small deviations in the Rayleigh-Jeans part, in agreement with Grimsrud & Wasserman (1998).

Time integrated observed spectrum of coasting photon thick outflow is broader than thermal one, and deviates from it both in low- and high-energy parts. This broadening is also found by Beloborodov (2010) using Monte-Carlo simulations, but our spectral index of the low energy part is $\alpha = 0$ instead of his $\alpha \simeq 0.4$. This difference may be attributed to the fact that Monte-Carlo simulations do not account for stimulated emission. Interestingly, we found $\alpha \simeq 0.34$ in the sharp photosphere approximation.

As discussed earlier in Section 3 each photon thick outflow always contains a photon thin layer with depth $\xi_{thin} = (R+l)/(2\eta^2)$ located near its outer boundary. Radiation diffused out from this part of the outflow arrives to observer first and modifies the initial part of the light curve and the corresponding spectrum of the outflow. The diffusion length

$\xi_D = [(R+l)^3/(\eta^2\tau_0 R_0)]^{1/2}$ remains always within this photon thin layer ξ_{thin} and our solution for photon thin outflow is applicable for description of this early emission. The photospheric emission from well developed photon thick outflow and its late time behavior occurring when the outflow crossed the photospheric radius may be described either by fuzzy or by sharp photosphere approximations.

When the outflow becomes transparent in the transition from photon thick to photon thin conditions, the observed time integrated spectrum will contain both Band component produced by the early emission from the photon thin layer and thermal-like component coming from the photon thick part superimposed. This may be the reason why in most GRBs analyzed by Ryde & Pe'er (2009) there are both power law and black body components.

We presented analytic expressions for the photon flux in the simple model of the portion of wind. With more complex density profile composed of presumably many shells the light curve is expected to be variable and arbitrarily complex. The minimal time scale of variability is given Eq. (29) and it may be very small for small baryon loading. It is necessary to emphasize that the decaying part of the light curve follows t_a^{-3} for photon thick outflows. Steeper decay of the light curve of photospheric emission it is a clear signature of the photon thin outflow.

The photospheric emission should be additionally identified by the spectral analysis. In particular, power law spectra extending to high energies above 10 MeV cannot be produced by the photospheric emission unless additional mechanisms are involved. What we have shown here, though, is that the observed spectrum may not necessarily be close to the thermal one.

8. CONCLUSIONS

In summary, in this paper we proposed a unified treatment of ultrarelativistic outflows, which originate both from instantaneous and from continuous energy release, with respect to photospheric emission. We have to stress that these two cases are discussed in the literature and are respectively referred to as shells and winds. Instead of this traditional division we propose a new physically motivated classification, which in our opinion helps to understand in particular why geometrically thin shell may appear as thick wind with respect to the photospheric emission. For this reason we re-examined the existing scattered literature and pointed out the advantage of the proposed classification.

We studied geometry of photospheres in generic relativistic outflows. As we are interested in appearance of the photosphere to a distant observer, we introduced the notion of photospheric equitemporal surface and described its dynamics.

We computed both energy flux and observed spectra of photon thick outflows in two approximations, derived from the radiative transfer equation. In our fuzzy photosphere approximation the effect of simultaneous emission from entire volume of the outflow is taken into account. We also used another computationally more simple sharp photosphere approximation which is shown to reproduces well both light curves and spectra. These results generalize the corresponding results in the literature for steady relativistic winds.

In photon thin outflows most of radiation is shown to originate not at its photospheric radius, but at smaller radii due to radiation diffusion. Starting from the radiative transfer equation for time dependent outflows we derived the diffu-

sion equation and obtained approximate analytic solution for the energy flux. We present both instantaneous and time integrated observed spectra. The latter are well described by the Band function. For our simple density profile we find values for the low energy power law index $\alpha = 1$ and the high-energy power law index $\beta \simeq -3.5$.

ACKNOWLEDGMENT

We thank the anonymous referee for useful remarks and suggestions.

REFERENCES

- Abramowicz, M. A., Novikov, I. D., & Paczynski, B. (1991). The appearance of highly relativistic, spherically symmetric stellar winds. *ApJ*, 369, 175–178.
- Aksenov, A. G., Ruffini, R., & Vereshchagin, G. V. (2007). Thermalization of Nonequilibrium Electron-Positron-Photon Plasmas. *Phys. Rev. Lett.*, 99(12), 125003–+.
- Aksenov, A. G., Ruffini, R., & Vereshchagin, G. V. (2009). Thermalization of the mildly relativistic plasma. *Phys. Rev. D*, 79(4), 043008.
- Aksenov, A. G., Ruffini, R., & Vereshchagin, G. V. (2010). Pair plasma relaxation time scales. *Phys. Rev. E*, 81, 046401.
- Band, D., Matteson, J., Ford, L., Schaefler, B., Palmer, D., Teegarden, B., Cline, T., Briggs, M., Paciesas, W., Pendleton, G., Fishman, G., Kouveliotou, C., Meegan, C., Wilson, R., & LeStrade, P. (1993). BATSE observations of gamma-ray burst spectra. I - Spectral diversity. *ApJ*, 413, 281–292.
- Beloborodov, A. M. (2010). Collisional mechanism for gamma-ray burst emission. *MNRAS*, 407, 1033–1047.
- Beloborodov, A. M. (2011). Radiative Transfer in Ultrarelativistic Outflows. *ApJ*, 737, 68–+.
- Bianco, C. L., Ruffini, R., & Xue, S. (2001). The elementary spike produced by a pure e^+e^- pair-electromagnetic pulse from a Black Hole: The PEM Pulse. *A&A*, 368, 377–390.
- Blinnikov, S. I., Kozyreva, A. V., & Panchenko, I. E. (1999). Gamma-ray bursts: When does a blackbody spectrum look non-thermal? *Astronomy Reports*, 43, 739–747.
- Couderc, P. (1939). Les aureoles lumineuses des Novaelig. *Annales d’Astrophysique*, 2, 271–+.
- Daigne, F. & Mochkovitch, R. (2002). The expected thermal precursors of gamma-ray bursts in the internal shock model. *MNRAS*, 336, 1271–1280.
- Giannios, D. (2006). Prompt emission spectra from the photosphere of a GRB. *A&A*, 457, 763–770.
- Goodman, J. (1986). Are gamma-ray bursts optically thick? *ApJ*, 308, L47–L50.
- Grimsrud, O. M. & Wasserman, I. (1998). Non-equilibrium effects in steady relativistic $e^+ + e^-$ -gamma winds. *MNRAS*, 300, 1158–1180.
- Haskell, R. C., Svaasand, L. O., Tsay, T.-T., Feng, T.-C., McAdams, M. S., & Tromberg, B. J. (1994). Boundary conditions for the diffusion equation in radiative transfer. *Journal of the Optical Society of America A*, 11, 2727–2741.
- Li, C. & Sari, R. (2008). Analytical Solutions for Expanding Fireballs. *ApJ*, 677, 425–431.
- Lyutikov, M. (2006). The electromagnetic model of gamma-ray bursts. *New Journal of Physics*, 8, 119–+.
- Maraschi, L. (2003). Jets at different scales. In S. Collin, F. Combes, & I. Shlosman (Eds.), *Active Galactic Nuclei: From Central Engine to Host Galaxy*, volume 290 of *Astronomical Society of the Pacific Conference Series* (pp. 275–+).
- Mészáros, P., Laguna, P., & Rees, M. J. (1993). Gasdynamics of relativistically expanding gamma-ray burst sources - Kinematics, energetics, magnetic fields, and efficiency. *ApJ*, 415, 181–190.
- Mészáros, P., Ramirez-Ruiz, E., Rees, M. J., & Zhang, B. (2002). X-Ray-rich Gamma-Ray Bursts, Photospheres, and Variability. *ApJ*, 578, 812–817.
- Mészáros, P. & Rees, M. J. (2000). Steep Slopes and Preferred Breaks in Gamma-Ray Burst Spectra: The Role of Photospheres and Comptonization. *ApJ*, 530, 292–298.
- Nakar, E., Piran, T., & Sari, R. (2005). Pure and Loaded Fireballs in Soft Gamma-Ray Repeater Giant Flares. *ApJ*, 635, 516–521.
- Paczynski, B. (1986). Gamma-ray bursters at cosmological distances. *ApJ*, 308, L43–L46.
- Paczynski, B. (1990). Super-Eddington winds from neutron stars. *ApJ*, 363, 218–226.
- Pe’er, A. (2008). Temporal Evolution of Thermal Emission from Relativistically Expanding Plasma. *ApJ*, 682, 463–473.
- Pe’er, A. & Ryde, F. (2011). A Theory of Multicolor Blackbody Emission from Relativistically Expanding Plasmas. *ApJ*, 732, 49–+.
- Pe’er, A., Ryde, F., Wijers, R. A. M. J., Mészáros, P., & Rees, M. J. (2007). A New Method of Determining the Initial Size and Lorentz Factor of Gamma-Ray Burst Fireballs Using a Thermal Emission Component. *ApJ*, 664, L1–L4.
- Piran, T. (1999). Gamma-ray bursts and the fireball model. *Phys. Rep.*, 314, 575–667.
- Piran, T. (2004). The physics of gamma-ray bursts. *Reviews of Modern Physics*, 76, 1143–1210.
- Piran, T., Shemi, A., & Narayan, R. (1993). Hydrodynamics of Relativistic Fireballs. *MNRAS*, 263, 861–867.
- Rees, M. J. (1966). Appearance of Relativistically Expanding Radio Sources. *Nature*, 211, 468–470.
- Rees, M. J. (1967). Studies in radio source structure-I. A relativistically expanding model for variable quasi-stellar radio sources. *MNRAS*, 135, 345–+.
- Ruffini, R., Aksenov, A., Bernardini, M. G., Bianco, C. L., Caito, L., Dainotti, M. G., de Barros, G., Guida, R., Vereshchagin, G., & Xue, S. (2009). The canonical Gamma-Ray Bursts: long, “fake”-“disguised” and “genuine” short bursts. In G. Giobbi, A. Tornambe, G. Raimondo, M. Limongi, L. A. Antonelli, N. Menci, & E. Brocato (Ed.), *American Institute of Physics Conference Series*, volume 1111 of *American Institute of Physics Conference Series* (pp. 325–332).
- Ruffini, R., Bianco, C. L., Chardonnet, P., Frascchetti, F., Vitagliano, L., & Xue, S. (2003). New perspectives in physics and astrophysics from the theoretical understanding of Gamma-Ray Bursts. In *AIP Conf. Proc. 668: Cosmology and Gravitation* (pp. 16–107).
- Ruffini, R., Bianco, C. L., Frascchetti, F., Xue, S.-S., & Chardonnet, P. (2001). On the Interpretation of the Burst Structure of Gamma-Ray Bursts. *ApJ*, 555, L113–L116.
- Ruffini, R., Salmonson, J. D., Wilson, J. R., & Xue, S.-S. (2000). On the pair-electromagnetic pulse from an electromagnetic black hole surrounded by a baryonic remnant. *A&A*, 359, 855–864.
- Ruffini, R., Vereshchagin, G., & Xue, S.-S. (2010). Electron-positron pairs in physics and astrophysics. *Physics Reports*, 487, 1–140.
- Rybicki, G. B. & Lightman, A. P. (1979). *Radiative processes in astrophysics*.
- Ryde, F. & Pe’er, A. (2009). Quasi-blackbody Component and Radiative Efficiency of the Prompt Emission of Gamma-ray Bursts. *ApJ*, 702, 1211–1229.
- Ryde, F., Pe’er, A., Nymark, T., Axelsson, M., Moretti, E., Lundman, C., Battelino, M., Bissaldi, E., Chiang, J., Jackson, M. S., Larsson, S., Longo, F., McGlynn, S., & Omodei, N. (2011a). Observational evidence of dissipative photospheres in gamma-ray bursts. *ArXiv e-prints*.
- Ryde, F., Pe’er, A., Nymark, T., Axelsson, M., Moretti, E., Lundman, C., Battelino, M., Bissaldi, E., Chiang, J., Jackson, M. S., Larsson, S., Longo, F., McGlynn, S., & Omodei, N. (2011b). Observational evidence of dissipative photospheres in gamma-ray bursts. *MNRAS*, 415, 3693–3705.
- Shemi, A. & Piran, T. (1990). The appearance of cosmic fireballs. *ApJ*, 365, L55–L58.
- Toma, K., Wu, X.-F., & Mészáros, P. (2011). Photosphere-internal shock model of gamma-ray bursts: case studies of Fermi/LAT bursts. *MNRAS*, 415, 1663–1680.

APPENDIX

For large opacities the distribution function of photons in comoving reference frame is close to isotropic one and the radiative diffusion approximation is accurate. Following Beloborodov (2011) we use spectral intensity in comoving frame $J_\nu(t, \xi, \mu)$. Starting from the radiative transfer equation (18) along the ray s in laboratory frame, we transform all variables except time t , depth ξ , and distance s into comoving reference frame

$$\nu^3 \frac{d}{ds} \left(\frac{J_\nu}{\nu^3} \right) = \frac{\kappa_\nu}{\mathcal{D}} (S_\nu - J_\nu), \quad (32)$$

and integrating over comoving frequency ν we have

$$\frac{1}{c} \frac{\partial J}{\partial t} - \frac{\mu}{\Gamma \mathcal{D}} \frac{\partial J}{\partial \xi} + \frac{1-\mu^2}{vt-\xi} \frac{\partial J}{\partial \mu} + 4 \frac{\Gamma \beta}{\mathcal{D}} \frac{1-\mu^2}{vt-\xi} J = \frac{\kappa}{\mathcal{D}} (S-J), \quad (33)$$

where $\mu = \cos \theta_c$, θ_c is the photon angle with respect to the radial direction in comoving frame, $\mathcal{D} = \Gamma(1 + \beta\mu)$ is Doppler factor, $J = \int J_\nu d\nu$ is total photon intensity, $S = \int S_\nu d\nu$ is total source function, $\kappa = J^{-1} \int \kappa_\nu J_\nu d\nu$ is effective opacity, $\kappa_\nu = \sigma n_c$ is opacity in comoving frame.

In the case of small deviations from isotropy decomposition

$$J = J_0(t, \xi) + \mu J_1(t, \xi) \quad (34)$$

could be applied. Introducing it into (33) and integrating it over $\mathcal{D} d\mu$ and over $\mathcal{D} \mu d\mu$ after some algebra for coherent scattering with $S = S_0 = J_0$ we have

$$\frac{\partial J_0}{\partial ct} + \frac{\beta}{3} \frac{\partial J_1}{\partial t} - \frac{1}{3\Gamma^2} \frac{\partial J_1}{\partial \xi} + \frac{2J_1}{3(vt-\xi)} + \frac{4J_0\beta}{3(vt-\xi)} = 0, \quad (35)$$

$$\frac{\partial J_1}{\partial ct} + \beta \frac{\partial J_0}{\partial t} - \frac{1}{\Gamma^2} \frac{\partial J_0}{\partial \xi} + \frac{8J_1\beta}{5(vt-\xi)} = -\frac{\kappa J_1}{\Gamma}. \quad (36)$$

Diffusion approximation is based on slow variation of total flux through the entire sphere $L_1 = J_1(t/t_0)^2$ over mean free path, so that $\frac{\partial L_1}{\partial ct} = 0$, and it provide J_1 from the equation (36). Inserting this into (35) after simple but tedious calculations in ultrarelativistic $\beta \simeq 1$ photon thin case $\Gamma^2 \xi \ll vt$ for function $L = J_0(t/t_0)^{8/3}$ we obtain the diffusion equation

$$\frac{\partial L}{\partial ct} - \frac{c^2 t^2 \Delta}{3R_0} \frac{\partial^2 L}{\partial \xi^2} = 0, \quad \Delta = \frac{1}{\Gamma^2 \tau_0}. \quad (37)$$

This equation should be supplemented with boundary conditions. There are two types of boundary conditions used frequently: free-streaming, for example in two-stream approximation (Rybicki & Lightman (1979), pp. 42–45), and zero boundary conditions, that can be used as replacement for free-streaming for "extrapolated boundary" (Haskell et al. 1994). We find that the position of "extrapolated boundary" $\xi = -k \frac{c^2 t^2 \Delta}{R_0}$ (k is a constant of order unity, dependent on the approximation used for free-streaming description) for the main part of emission is very close to the real boundary, and in the case of zero boundary conditions $L|_{\xi=0} = L|_{\xi=l} = 0$ there is a series expansion of solution, that for initial conditions $L(\xi, t_0) = 1$ gives

$$L(\xi, t) = \sum_{n=0}^{\infty} \frac{4}{(2n+1)\pi} \exp \left[-\frac{\Delta(2n+1)^2 \pi^2 c^3 (t^3 - t_0^3)}{9R_0 l^2} \right] \sin \left[\frac{(2n+1)\pi \xi}{l} \right]. \quad (38)$$

This solution in comparison with numerical one with free-streaming boundary conditions is accurate to a few percents.

The flux of L is characterized by an initial burst and then tends to the asymptotic solution, that corresponds to $t_0 = 0$, with flux

$$F(t) = \frac{4\Delta c^3 t^2}{3R_0 l^2} \vartheta_2 \left[0, \exp \left(-\frac{4\Delta \pi^2 c^3 t^3}{9R_0 l^2} \right) \right], \quad (39)$$

where ϑ_2 is the Jacobi elliptic theta function, see Fig. 13. The peak of the flux of L is near the diffusion time

$$t_D = \frac{l}{c} \left(\frac{R_0}{l\Delta} \right)^{1/3}, \quad (40)$$

and "extrapolated boundary" $\xi = -kl(l\Delta/R_0)^{1/3} \ll l$ is very close to real one as $\Delta \ll 1$, that ensures the accuracy of (38).